ARTICLE OPEN

Check for updates

Electrochemical characterization and degradation of carbon fibre reinforced polymer in quiescent near neutral chloride media

Stanley Udochukwu Ofoegbu[1,2]✉, Marcela C. Quevedo[2], A. C. Bastos[2], M. G. S. Ferreira[2] and M. L. Zheludkevich[3,4]

In a quest for a better understanding of the mechanism and contribution(s) of fresh ("un-degraded") and degraded CFRP surfaces to galvanic corrosion of coupled metals in multi-material assemblies the electrochemical behaviour of CFRP in quiescent 50 mM NaCl was studied using electrochemical techniques. Tests using ferricyanide/ferrocyanide redox couple revealed a quasi-reversible behaviour. Under cathodic polarization, CFRP is active electrochemically evidenced by the increase in pH (to pH ≥ 10). Galvanic current densities and potentials for Al-CFRP couple comprised of freshly polished CFRP sample ranged from 15–25 μA cm^{-2} and ≈−660 to −850 mV_{SCE} respectively, while the corresponding parameter for Al-CFRP couple comprised of degraded CFRP were in the range 10–25 μA cm^{-2} and ≈−670 to −900 mV_{SCE}. Contrary to expectations, CFRP prior exposure to degradative high pH media before galvanic coupling did not result in an increase in the intensity of galvanic corrosion of the coupled metal.

npj Materials Degradation (2022)6:49 ; https://doi.org/10.1038/s41529-022-00261-1

INTRODUCTION

Carbon fibre-reinforced polymers (CFRPs) are widely used as components of high-performance hybrid structures. In the transport industry (automobile and aerospace) where weight reduction with improved strength is driving designs, CFRPs are used and can come in contact with metallic members. Whereas the electrochemical behaviour of the more active metallic constituents of these hybrid structures are well known, the same is not true about CFRPs, which are usually considered inert components in such multi-material structures. When coupled with metals and alloys CFRP is capable of promoting galvanic corrosion by supporting cathodic reactions[1,2]. Since CFRP is cathodically polarized on contact with most structural metals and alloys, an understanding of its electrochemical behaviour at such potentials is vital to mitigating galvanic corrosion in hybrid structures comprising CFRPs. On galvanic coupling to zinc, aluminium, and iron in near-neutral aqueous chloride media (50 mM NaCl), CFRP has been observed to be cathodically polarized to about −1000 mV_{SCE}, −660 to −750 mV_{SCE}, and −330 to −500 mV_{SCE} respectively from its OCP value[3]. This cathodic polarization of conductive composites when in contact with metals has been reported to enhance corrosion of the metallic members[4–6]. Cathodic polarization of conductive composites is also reported to enhance the degradation of certain polymer composites especially those with polymer matrices capable of ring-opening reactions in the presence of hydroxyl and peroxide ions[7–10], as a consequence of the cathodic reactions on the conductive polymer composites. However, epoxy composites are reported to be more resistant to this polymer degradation mechanism[10]. Anodic polarization of CFRPs which could result from stray electrical currents has been reported to be capable of causing fast and significant corrosion damage at applied current densities as low as 1 μA cm^{-2}[11].

Carbon fibre reinforced composite materials and high-performance alloys are presently frequently used in multi-material combinations. Cathodic polarization of carbon fibre reinforced polymer composites either by galvanic coupling or by an impressed cathodic polarization has been demonstrated to be capable of leading to some degradation of the polymer composite[1,3,5,6,8–10,12–17].

Generally, the double-layer capacitance of carbon materials had been reported to be about ≤20 μF cm^{-2}[18]. Kinoshita[19] reported that in aqueous electrolytes carbon surfaces exhibit a double-layer capacitance of 10–20 μF cm^{-2}. Frackowiak and Beguin[20] reported 15–50 μF cm^{-2} for the range of values of the capacitance of carbon materials, and 25 μF cm^{-2} as the average value. However, the actual values of double-layer capacitance of carbon surfaces are reported to be dependent on the type of carbon and its method of preparation[20]. In addition, various reports have confirmed differences in the electrochemical activity of edge plane and basal sites on carbon materials[21–23]. Randin and Yeager[24] reported significant differences in the double layer capacitances of the basal and edge sites of graphite; with capacitance values of 3–16 μF cm^{-2} attributed to the basal sites, and 50–70 μF cm^{-2} to the edge sites, based on results of tests in 0.9 M NaF solutions. Yuan et al.[23], studied the electrochemical behaviour at single-layer graphene-based electrodes, compared the basal plane of graphene to its edge plane, and reported faster electron transfer kinetics on the edge plane coupled with four orders of magnitude increase in specific capacitance, and stronger electrocatalytic activity relative to graphene basal plane. The production processes for carbon fibres appear to favour the preponderance of the more electrochemically active edge sites on its ends (the transverse cross-sections employed in this study).

It is worthy to note that besides the unidirectional and transverse presentation of carbon fibres in the CFRP surface used

[1]Centre for Mechanical Technology and Automation (TEMA), Department of Mechanical Engineering, University of Aveiro, Campus Universitário de Santiago, 3810-193 Aveiro, Portugal. [2]Department of Materials and Ceramic Engineering, CICECO-Aveiro Institute of Materials, University of Aveiro, Campus Universitário de Santiago, 3810-193 Aveiro, Portugal. [3]Institute of Surface Science, Helmholtz-Zentrum Hereon, Max-Planck-Strasse 1, 21502 Geesthacht, Germany. [4]Institute for Materials Science, Faculty of Engineering, Kiel University, Kiel 24103, Germany. ✉email: ofoegbu.stanley@ua.pt

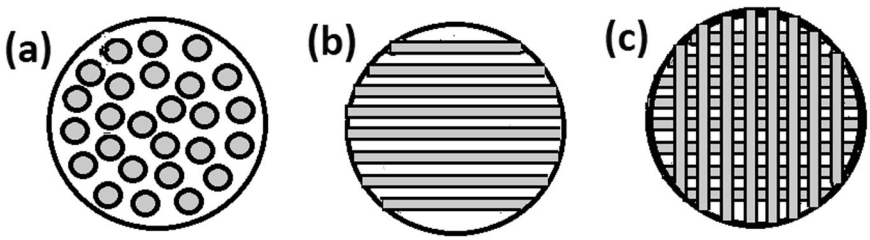

Fig. 1 Various presentations of carbon fibers on the CFRP surface. Different possible presentations of carbon fibres on CFRP surface, **a** unidirectional with fibre ends exposed, **b** unidirectional with fibre length exposed, and **c** a weave with fibre lengths exposed (carbon fibres are grey while polymer matrix is white).

in this work (Fig. 1a) which favours a preponderance of edge sites, CFRP surfaces can present carbon fibres in a variety of ways (Fig. 1b and c) which might favour preponderance of basal sites with consequent implications on electrochemical activity; most probably reduced electrochemical activity.

This work aims at a better understanding of the electrochemical behaviour of CFRP and its effects/contribution(s) to enhanced galvanic corrosion of coupled metals in multi-material assemblies, and its degradation under such (galvanic corrosion) conditions. To achieve these aims, first, cyclic voltammetric tests using the ferricyanide/ferrocyanide redox couple were employed to study the electrode properties of CFRP and gain some insight regarding the magnitude of the electrochemically active area. Next, data on its open circuit potential profile, its response to potentiodynamic polarization, changes in the local pH near CFRP during cathodic polarization, and its impedance spectra were acquired in repeated tests. To validate data from impressed polarization tests on CFRP, galvanic current densities and potentials, and the pH profile 40 µm above the CFRP surface was determined using an Al-CFRP couple in quiescent 50 mM NaCl.

In order to predict the magnitude(s) of possible anodic dissolution rates of metals galvanically coupled to CFRP (the cathode in such galvanic couples), knowledge of the magnitude of the cathodic current densities that can be generated on CFRP surface at cathodic potentials consistent with values it is polarized to in requisite galvanic system(s) is necessary. Consequently, these parameters were determined in this work. Furthermore, the effect of prior composite degradation on galvanic corrosion of coupled metal is established and compared with trends observed for metal coupled to fresh CFRP surface (with no prior degradation).

RESULTS

Results overview

The results from experimental activities are presented in this section followed by brief discussions of these results while the implications on the use of CFRP in combination with metals is addressed in the ensuing discussion section. First, results from tests to determine the electrode properties of CFRP and its surface area are presented. This was based on OCP measurements, EIS at OCP, and cyclic voltammetry with a redox couple. Secondly, results that depict the electrochemical behaviour of CFRP and changes in its local environment under impressed polarization are presented. Finally, results demonstrating the long-term effects of observed changes due to polarization (surface evolution, and pH changes) on the degradation of CFRP and coupled metal(s) are presented.

Initial electrochemical characterization of CFRP

OCP profile of CFRP from duplicate measurements in 50 mM NaCl (Fig. 2) shows a general trend of a drift to more anodic values in the range of 75–175 mV_{SCE} during 10 h. It is noteworthy that the

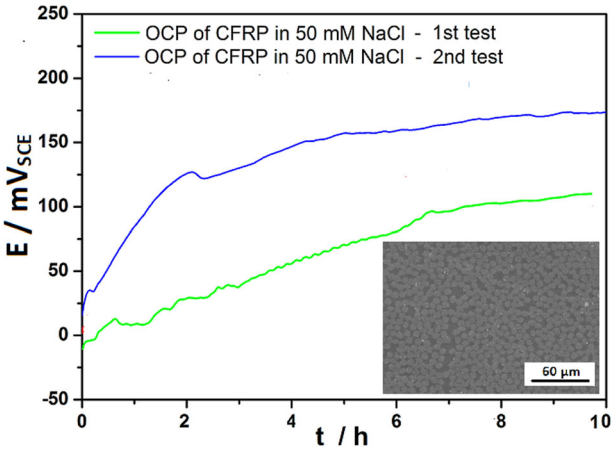

Fig. 2 Open circuit potential of CFRP. Open circuit potential profile for CFRP in 50 mM NaCl (inset is a low magnification SEM image of CFRP surface prior to immersion).

observed apparent fluctuation(s) in the OCP profiles of CFRP on repeated measurements in the test media is similar to fluctuations observed on repeated measurements of OCP profiles of active metals. This trend is sustained in repeated OCP measurements with differences in exact measured values with time varying within the range of ±75 mV. A comparison of the OCP profile for CFRP in 50 mM NaCl with OCP profile of six common engineering metals (Cu, Sn, Fe, Al, Zn, and Mg) in the same media indicates that CFRP is consistently anodic to these metals (See Supplementary Fig. 1) and indicates the potentials CFRP can be polarized to on galvanic coupling to these metals in the test media.

Six repeated measurements of the electrochemical impedance spectra of CFRP in 50 mM NaCl solution were acquired (See Supplementary Fig. 2) and fitted with a one-time constant equivalent circuit (inset in Fig. 3a) to determine the values and range of variability on repeated tests of such important electrochemical parameters as polarization resistance/charge transfer resistance (R_p/R_{ct}) and double-layer capacitance (C_{dl}), and low-frequency impedance.

Capacitances were calculated from impedance data using the relation (Eq. 1) proposed by Brug et al.[25];

$$C = Y_o^{\frac{1}{n}} \cdot \left[\frac{1}{R_s}\right]^{\frac{n-1}{n}} \quad (1)$$

where Y_o is the fitted value of CPE element, R_s is the resistance in series with a CPE element (in this case, the solution resistance) and n is the CPE exponent.

From the acquired impedance spectra (Supplementary Fig. 2) the reproducibility or close similarities in the spectra acquired from different tests can be appreciated. Determination of the values of these electrochemical parameters are of great importance as these values are the baseline for monitoring and

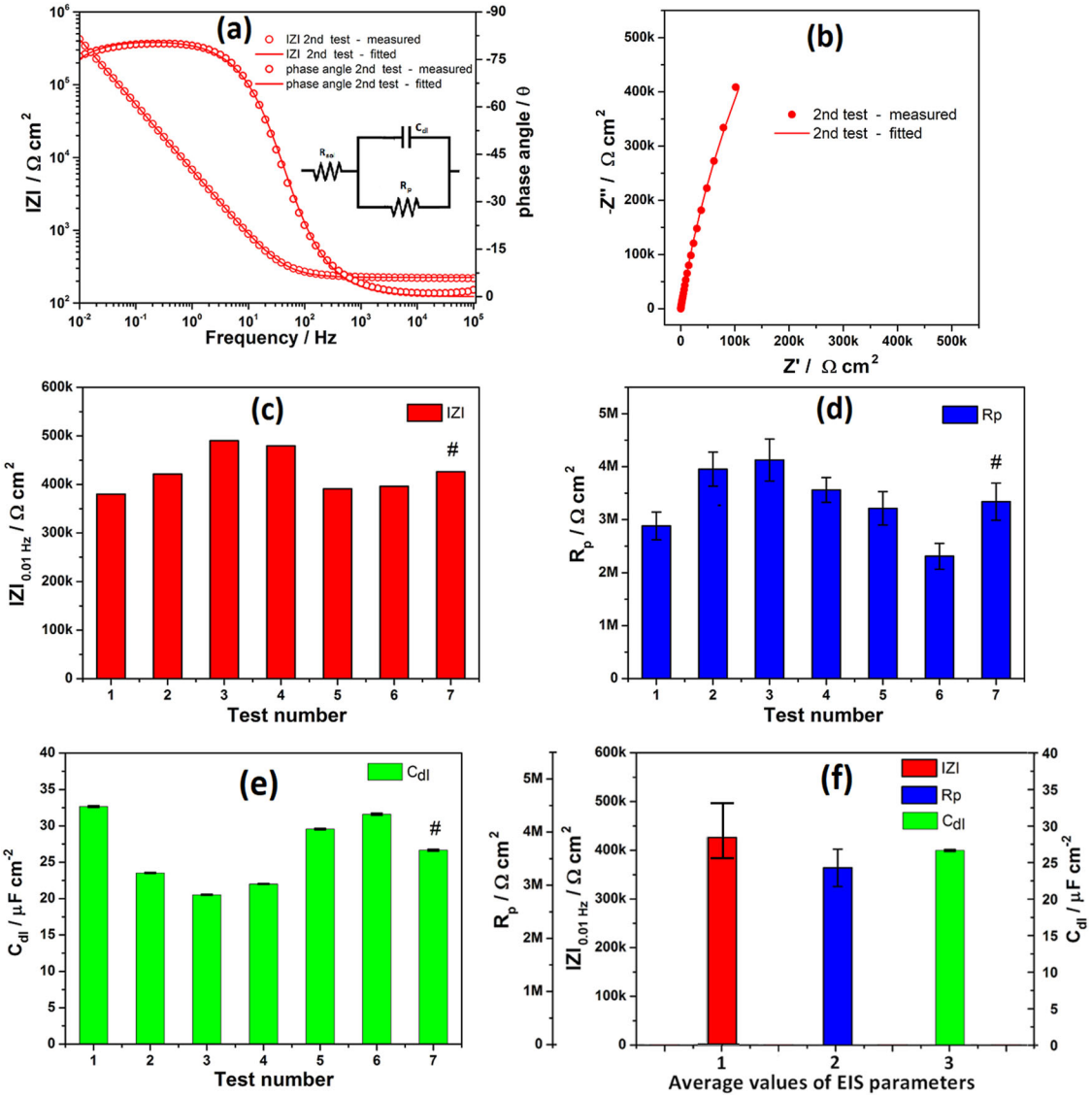

Fig. 3 EIS spectra of CFRP at OCP. Measured and fitted impedance spectra, and fitted parameters for each of the hextuple EIS tests on CFRP in 50 mM NaCl after 1 h immersion at OCP, **a** representative Bode plot (log impedance modulus and phase angle, inset is equivalent circuit used to fit impedance spectra), **b** representative Nyquist plot, **c** measured low-frequency impedance (at $|Z|_{0.01\ Hz}$), **d** fitted polarization resistance, **e** calculated double-layer capacitance (Test number 7 and # denote the mean values from six measurements), and **f** mean values of EIS parameters (from hextuple measurements).

evaluating the effects of applied potential(s), changes in pH, presence of inhibitors, polymer degradation etc., on the electrochemical behaviour of CFRP that will be the focus of subsequent communications. From analysis of hextuple measured and fitted EIS data (representative spectra presented as Bode and Nyquist plots respectively in Fig. 3a and b) acquired from CFRP without "applied" polarization in quiescent 50 mM NaCl solution, the range of the values of low-frequency impedance is determined to be 0.38–0.49 MΩ cm^2 (Fig. 3c and f), the polarization resistance 2.88–4.22 MΩ cm^2 (max. fitting error ≈ 10.5%) (Fig. 3d and f), and double-layer capacitance 20.54–32.66 μF cm^{-2} (max. fitting error ≈ 0.46%) (Fig. 3e and f).

For a better understanding of the electrode properties of CFRP cyclic voltammetry study of the electrode behaviour of CFRP was carried out at different scan rates using the well-known ferricyanide/ferrocyanide redox couple, (0.1 M KCl + 1 mM $K_4[Fe(CN)_6]$ + 1 mM $K_3[Fe(CN)_6]$), and the results presented as Fig. 4 and Table 1. From the acquired cyclic voltammograms (Fig. 4a) it is obvious that both peak currents increased with increase in the scan rates. Capacitive response appears to predominate at increased scan rates (>100 mV s^{-1}) at the expense of faradaic processes. This is most likely due to limited time being available for charge transfer reactions to flourish during one scan cycle. This can be observed in the increase in discrepancies in the anodic peak currents and cathodic peak currents from scan rates beyond 100 mV s^{-1} (Fig. 4 and Table 1).

To determine the exact relationships between the peak currents and the scan rates and gain further insight on the electron transfer behaviour on CFRP surface in the presence of this redox couple, a plot of the modulus of both the anodic ($I_{p,a}$) and cathodic ($I_{p,c}$) peak currents against the square root of the corresponding scan rates were made and presented in Fig. 4b.

From Table 1, it can be observed that the peak-to-peak separation (ΔE) increases with increasing scan rate which is indicative of a quasi-reversible electrochemical process[26]. For fast electron transfer processes, the peak-to-peak separation (ΔE) would be insensitive to increasing scan rates.

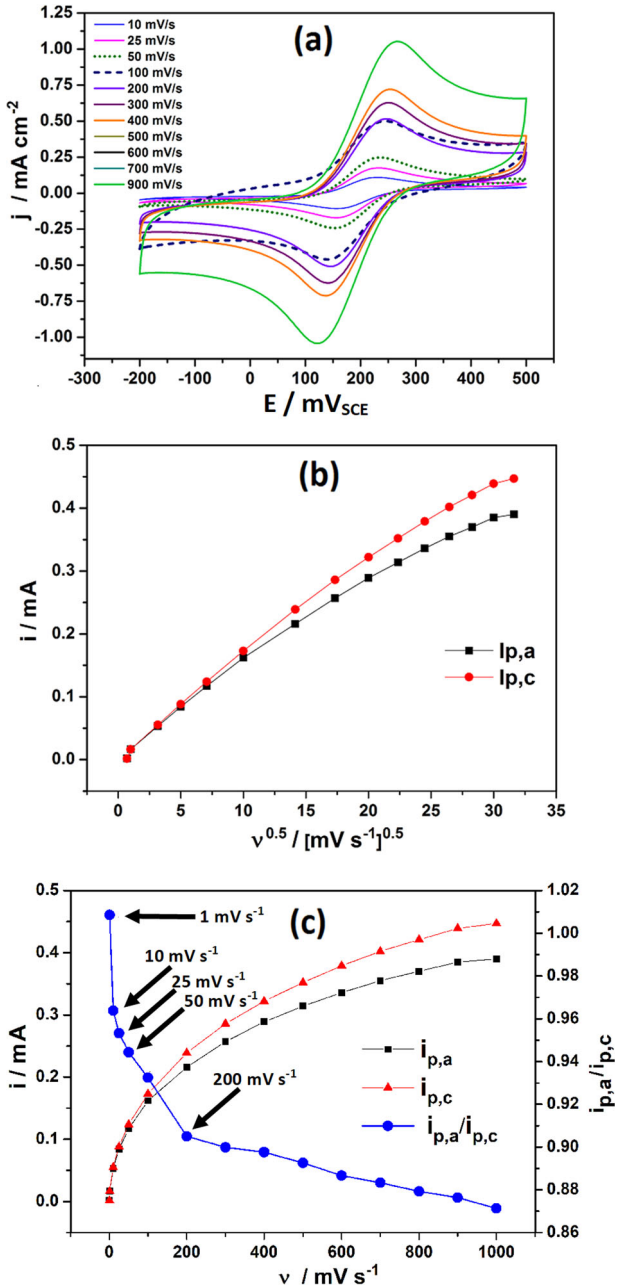

Fig. 4 Cyclic voltammetry data of CFRP. Cyclic voltammetry data of CFRP in 0.1 M KCl + 1 mM $Fe[(CN)_6]^{3+}$ + 1 mM $Fe[(CN)_6]^{4+}$at different scan rates, **a** cyclic voltammogram of CFRP from 10 to 900 mV s^{-1}, **b** plot of modulus of peak currents vs. $v^{1/2}$(√ of scan rate) for CFRP in 0.1 M KCl + 1 mM $Fe[(CN)_6]^{3+}$ + 1 mM $Fe[(CN)_6]^{4+}$, **c** plot of modulus of peak currents and ratio of anodic to cathodic currents ($i_{p,a}/i_{p,c}$) vs. v (scan rate) for CFRP in 0.1 M KCl + 1 mM $Fe[(CN)_6]^{3+}$ + 1 mM $Fe[(CN)_6]^{4+}$ respectively.

Using the Randles-Sevcik equation (Eq. 2) and the well-reported diffusion coefficient of ferrocyanide in 0.1 M KCl (7.20×10^{-6} cm^2 s^{-1}), the electrochemically active surface area was calculated at different scan rates and presented in Table 1.

$$i_p = \left(2.69 \times 10^5\right) n^{3/2} A D^{1/2} C v^{1/2} \quad (2)$$

where n is equal to the number of electrons gained/lost in the reduction/oxidation process, A is the surface area of the working electrode in cm^2, D is the diffusion coefficient in cm^2 s^{-1}, v is the sweep rate in V s^{-1}, and C is the molar concentration of the active specie(s) in the bulk solution.

From reviewing the literature, we infer that by optimizing the size of the microelectrodes in a microelectrode array, the distance between neighbouring microelectrodes, and the scan rate, a scenario can be obtained in which interaction (overlapping) of diffusion zones between neighbouring electrodes is avoided; resulting in a sustained radial diffusion front over each microelectrode[27–32]. Such a scenario could result in enhancement of electrochemical activity to values several times higher than that from a macroelectrode of similar geometric surface area experiencing a planar diffusion field. Thus, the CFRP can be perceived to act as a microelectrode array (MEA) comprised of conductive 6-micron diameter carbon fibres dispersed in non-conducting epoxy matrix. This inferred enhancement of the electrochemically active surface area (EASA) of the CFRP sample is principally attributed to the "microelectrode(s) effect" in which the 6 µm diameter carbon fibres being dispersed on the composite surface act as a distinct array of microelectrodes. Such increase in current output in microelectrode array assemblies has been exploited in the design of a variety of sensors for several applications[33–43].

Electrochemical behaviour of CFRP under polarization

The effect of impressed polarization (at mainly cathodic potentials) on CFRP in quiescent 50 mM NaCl was studied systematically using a wide array of electrochemical techniques (cyclic voltammetry, potentiodynamic polarization, chronoamperometry at fixed and stepped potentials respectively, scanning vibrating electrode technique (SVET)), and electrochemical impedance spectroscopy (EIS) under impressed potential(s), separately and in galvanic couples, and the results presented herein.

By a step-wise change in the potential applied to CFRP in quiescent 50 mM NaCl from −1000 mV_{SCE} to 500 mV_{SCE} and holding the potential constant for some minutes before changing the potential (in steps of 250 mV) while simultaneously monitoring the local pH (Figs. 5 and 6), it is observed that the local pH near CFRP is sustained at values ≥9.5 up to an applied potential of −500 mV_{SCE}. As the potential is stepped the local pH changes drastically tending towards values significantly different from values in the bulk solution. This trend indicates that alkalinization of the local pH near CFRP on the galvanic coupling to metals will be very significant on the galvanic coupling to zinc ($E_{corr} \approx -1000$ mV_{SCE}), and aluminium ($E_{corr} \approx -650$ to -850 mV_{SCE}), and much less marked with iron ($E_{corr} \leq -500$ mV_{SCE}) in 50 mM NaCl (Supplementary Fig. 2)[3]. Consequently, an understanding of the effects of changes in pH on the electrochemical behaviour of CFRP is important and merits further study.

On changing the way in which the applied potential is varied from big potential steps (250 mV steps) over longer times (Fig. 5) to a linear scan from −1500 to +1500 mV_{SCE} using a step size of 1 mV and scan rate 1 mV s^{-1} (Fig. 6) while monitoring the local pH, the same trends are observed in variation of local pH near CFRP surface with changes in the applied potential.

Cyclic voltammograms of CFRP during 10 cycles in 100 ml of 50 mM NaCl at a scan speed of 10 mV s^{-1} was acquired and the first one is shown in Fig. 7. This voltammogram is distinguished by the presence of two close cathodic peaks without any corresponding anodic peaks during the reverse scans. These phenomena indicate that the specie(s) (reactants and products) involved in these processes most probably do not persist on the electrode surface to be oxidized on the reverse scan. The more prominent peak around −300 mV_{SCE} is attributed to the 2-electron reduction of oxygen to the hydroperoxyl (HO_2^-) ion to hydroxyl ion (OH^-) (Eq. 3)[44–46].

$$O_2 + H_2O + 2e^- \rightleftharpoons HO_2^- + OH^- (E_o \approx -309\ mV_{SCE}). \quad (3)$$

Table 1. Parameters from cyclic voltammograms in ferricyanide/ferrocyanide redox couple.

Scan rate (mV s^{-1})	Scan rate (V s^{-1})	Ep_1 (mV)	Ep_2 (mV)	ΔE (mV)	$((Ep_1+Ep_2)/2)$ (mV)	Ip_1 (A)	Ip_2 (A)	EASA (cm^2)
1	**0.001**	**224**	**161**	**63**	**192.5**	**1.66E−05**	**1.64E−05**	**1.29**
10	**0.01**	**221**	**161**	**60**	**191**	**5.33E−05**	**5.53E−05**	**1.26**
25	**0.025**	**228**	**159**	**69**	**193.5**	**8.40E−05**	**8.82E−05**	**1.27**
50	**0.05**	**230**	**155**	**75**	**192.5**	**1.17E−04**	**1.24E−04**	**1.29**
100	**0.1**	**234**	**153**	**81**	**193.5**	**1.62E−04**	**1.73E−04**	**1.32**
200	0.2	242	149	93	195.5	2.16E−04	2.39E−04	1.39
300	0.3	246	145	101	195.5	2.57E−04	2.86E−04	1.44
400	0.4	248	141	107	194.5	2.89E−04	3.22E−04	1.47
500	0.5	250	137	113	193.5	3.14E−04	3.52E−04	1.52
600	0.6	254	131	123	192.5	3.36E−04	3.79E−04	1.56
700	0.7	254	131	123	192.5	3.55E−04	4.02E−04	1.59
800	0.8	258	129	129	193.5	3.70E−04	4.21E−04	1.63
900	0.9	258	127	131	192.5	3.85E−04	4.39E−04	1.66
1000	1	266	121	145	193.5	3.90E−04	4.47E−04	1.73

Bold values are for the frequently used scan rate range (1–100 mV s^{-1}).

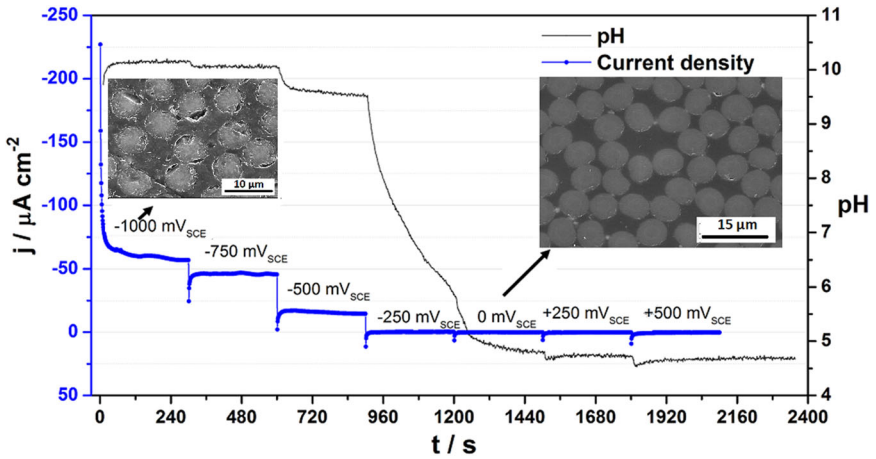

Fig. 5 pH and current density profiles on CFRP subjected to stepped polarization. Measured pH and current above CFRP in 50 mM NaCl with step-wise change in applied polarization (all potentials are measured versus saturated calomel electrode).

Electrochemical impedance spectroscopy was employed to probe the observed variation in the electrochemical activity of CFRP with impressed potential over a very wide potential range (from −1500 to +1500 mV_{SCE}) and selected Bode plots presented as insets 1–8 in Fig. 7. Comprehensive EIS data acquired in this wide potential range are presented as Supplementary Fig. 3. Calculations of capacitance were made from tests carried out at OCP (Fig. 3).

EIS results at different impressed potentials (presented as insets 1–8 in Fig. 7 and Supplementary Fig. 3) show that smaller cathodic polarization (−250 and −500 mV_{SCE}), that are less negative than the range observed for Al-CFRP couple in the test media (Fig. 13) resulted in a greater decrease in the total impedance of the CFRP compared to measurements at OCP (+120 mV_{SCE}), −750 mV_{SCE}, and even −1000 mV_{SCE}. From Fig. 7 (and Supplementary Fig. 3), it is obvious that only an anodic polarization of +1000 mV_{SCE} caused a reduction in the total impedance below that measured at OCP. Correlating the measured total impedance at low frequency (0.01 Hz), with the applied potential (Supplementary Fig. 3), it is observed that whereas an increase in cathodic applied potential resulted in an increase in the impedance of the system, the reverse was mostly the case on anodic polarization, though the impedance on anodic polarization was always higher than that for same cathodic polarization at same time interval. In a one-time constant system, increase in total impedance means that the resistance to charge transfer across this interface has increased.

Since, over the very wide potential range tested, a variety of processes appear to be involved at the different potential ranges (Fig. 7 and Supplementary Fig. 3), a robust treatment of the impedance spectra was carried out to deconvolute and extract the respective parameters using the equivalent circuit shown in Fig. 8. The second time constant appearing at the low frequencies (Fig. 7 and Supplementary Fig. 3) as soon as impedance drops, are postulated to be related to diffusion control at cathodic polarization. To confirm this, EIS spectra were acquired in steps of 25 mV from +250 to −500 mV_{SCE} (Fig. 9) and fitted to the two-time constant equivalent circuit presented in Fig. 10.

This potential range was chosen because it encompasses the "E_{corr}" and extends up to the diffusion-limited regime of CFRP immersed in quiescent 50 mM NaCl solution. Bode plots obtained in this potential range (between +250 and −500 mV_{SCE}) are presented in Fig. 9 and the parameters extracted from fitting the EIS spectra in Fig. 10.

Since charges need to be passed for CFRP to support the anodic dissolution of metals it might be galvanically coupled with in multi-

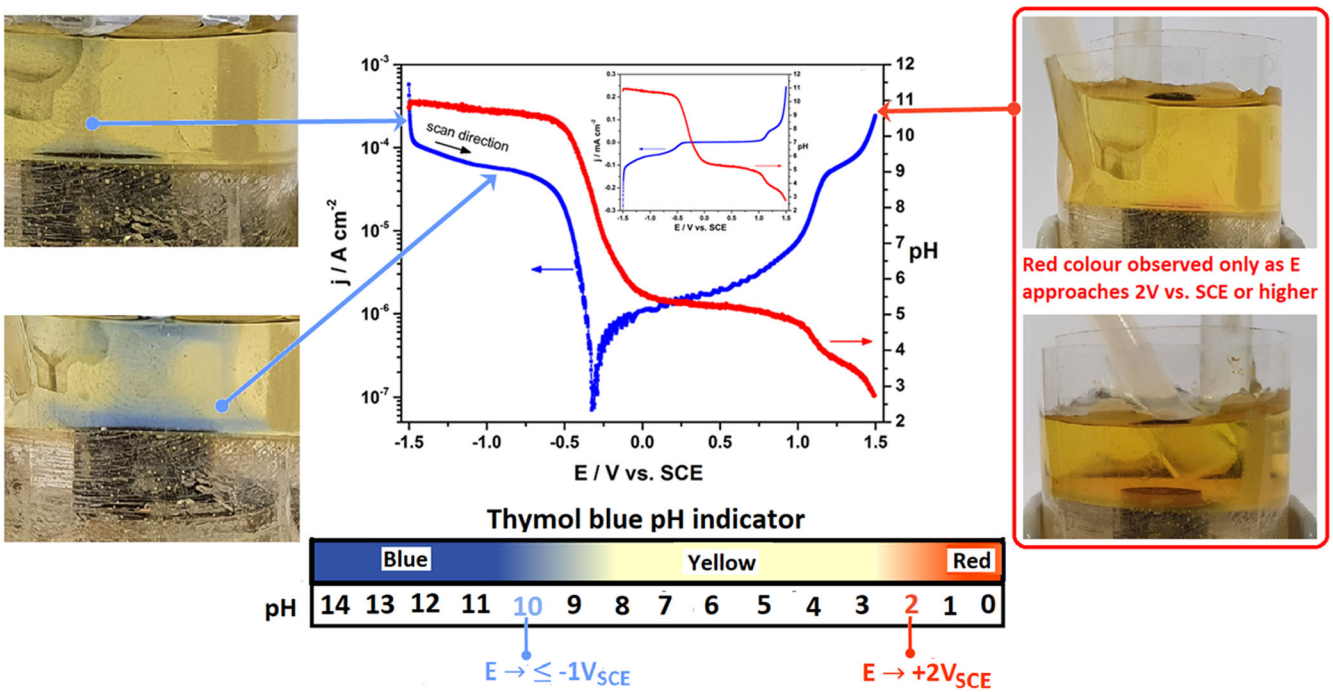

Fig. 6 pH and current density profiles on CFRP subjected to linear polarization. pH profile of CFRP in 50 mM NaCl measured simultaneously with polarization from −1500 to +1500 mV_{SCE} using a step size of 1 mV and scan rate 1 mV s^{-1}. (Inset is a linear plot of the same data, and pictures indicate changes in solution colour in the presence of thymol blue pH indicator at different polarizations).

material combinations, such a scenario was simulated by polarizing CFRP to different cathodic potentials that are relevant to galvanic coupling to a range of metals, and the current profile monitored during 4 h. Triplicate tests were carried out at each potential, and the results were statistically analysed using Graphpad Prism software (version 6). Integration of the current(s) passed during this duration enabled evaluation of the charges passed at the different impressed potentials (Fig. 11, Supplementary Tables 1 and 2). Employing one-way analysis of variance and Dunnett's Multiple Comparison test of datasets with a significant difference set at ($P < 0.05$) for each polarization potential against the dataset for quantity of charges passed at 0 mV_{SCE} polarization (closest to OCP values in test solution) confirms that the quantity of charges passed become quite significant at potentials more negative than −125 mV_{SCE} (Fig. 11, Supplementary Tables 1 and 2).

Polarization effect on degradation of CFRP and coupled metal

Results confirming the changes in local environment and effects of polarization and prior composite degradation on galvanic corrosion of coupled metal under realistic polarization scenarios are presented. Results of the pH profile measurements across Al and CFRP galvanically coupled and uncoupled in 50 mM NaCl at 12 µm from the surfaces confirm intense cathodic activity on CFRP polarized by coupling galvanically to aluminium (−650 to −850 mV_{SCE}), evidenced by the increase in pH over the CFRP on coupling (Fig. 12a).

Locally generated electric field(s) are known to affect the response of ion-selective electrodes used to detect relevant ions/species in corroding systems[47–50]. This effect can lead to either under estimation or over estimation of the measured potential signal in galvanic systems due to plausible contributions of the electric field (generated due to galvanic coupling) to the measured potential in potentiometric tests[50]. Bringing the reference and measuring electrodes very close together so the electric field experienced by both become equal and thus cancel out, or use of an electric relay as a switch between the galvanic couple that disconnects them for a very short period of time, while the measurement is being carried out have been proposed as a viable solution to minimizing the effect of the electric field[50]. In the light of these, efforts were made to clarify the fidelity of the pH profiles measured across Al-CFRP couple (Fig. 12a) and on CFRP under impressed polarization (Figs. 5 and 6) by measuring the pH using a pH-sensitive microelectrode and the potential due to the electric field using a reference microelectrode. The reference microelectrode is similar to the pH microelectrode but without the sensitive gel at the tip. From Fig. 12b, it can be observed that while the pH electrode sensed a voltage variation of around 400 mV during the polarization sweep, the micro-reference electrode (sensing the electric field) sensed only 2 mV variation. This means that the effect of the potential drop in solution is negligible; and hence the pH values measured in this work are really from pH changes and not artefacts due to other sources of potential in solution.

To show the trends in repeated galvanic corrosion measurements results of duplicate measurements of the galvanic current density, measured by zero resistance ammetry, and galvanic potentials across freshly polished CFRP samples coupled to high purity aluminium are presented (as Supplementary Fig. 4 and Fig. 13), and enabled us to determine values for these important parameters to be in the range of 15–25 µA cm^{-2} and ≈−660 to −850 mV_{SCE} respectively in quiescent 50 mM NaCl. On the strength of perspectives gained from an earlier treatise[51] on galvanically stimulated degradation of CFRP composites we sought to also gain insight on how prior degradation of CFRP in multi-material assemblies might affect galvanic corrosion of (newly) coupled metallic materials by comparing the galvanic current density profile of fresh CFRP surface coupled to metal (Fig. 13b) and CFRP surface that had gone through prior degradation (due to 592 h exposure to pH 11 buffer solution) prior to coupling to fresh metal surface (red line in Fig. 13).

DISCUSSION

The values of double-layer capacitance reported in this work for CFRP (20.54–32.66 µF cm^{-2}) compares favourably with values of 15–50 µF cm^{-2} reported by Frackowiak and Beguin[20] as well as

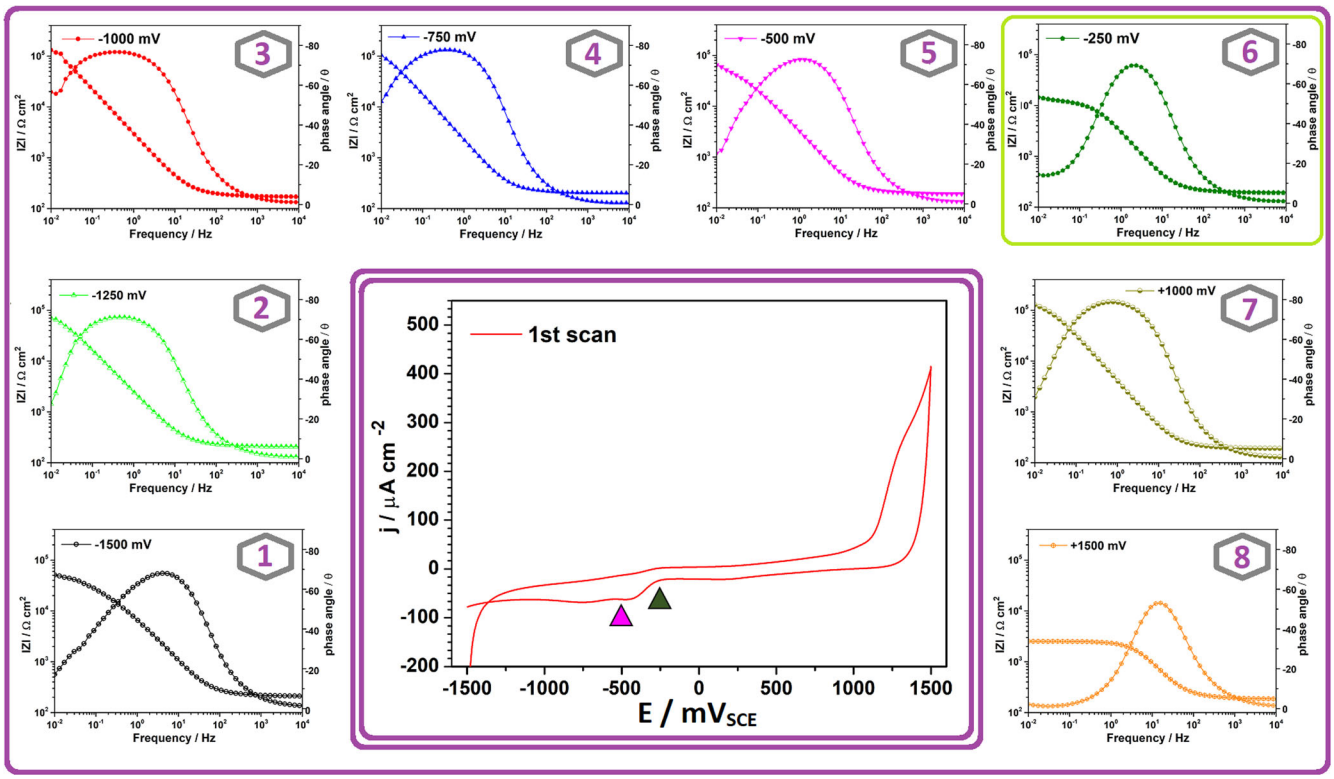

Fig. 7 Cyclic voltammogram of CFRP with EIS data at different polarizations. Cyclic voltammogram of CFRP during 10 cycles (1st scan) in 50 mM NaCl at a scan speed of 10 mV s^{-1} (Insets 1–8 are EIS spectra in Bode plot format at cathodic and anodic potentials of interest).

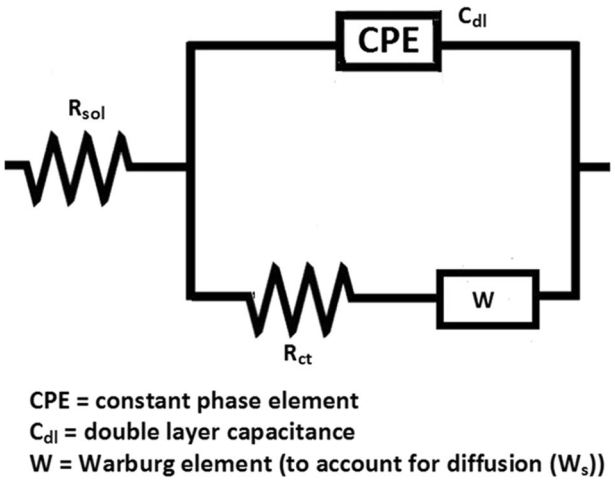

Fig. 8 Equivalent circuit. Equivalent circuit used to fit impedance spectra in order to evaluate diffusion control effects.

the average value of 25 μF cm^{-2} suggested for carbon surfaces by Frackowiak and Beguin[20] in spite of the fact that the geometrical carbon surface area is (about 35%) lower in the case of CFRP composite than that of a "non-composite" carbon surface. Accounting for this lower geometrical carbon surface area in CFRP, places the capacitance of the carbon surface fraction of CFRP in the higher end of the range suggested for carbon surfaces by Frackowiak and Beguin[20]. The high values of polarization resistance/charge transfer resistance ≈ ≥2 MΩ cm^2 (Fig. 3d) might be indicative of a high resistance to faradaic processes or charge transfer across the CFRP-solution interface.

Based on calculated values of capacitance from EIS data (both individual and average value) it is concluded that the transverse sections (ends) of the carbon fibres of the CFRP are predominated by graphite edge sites as the individual (20.54–32.66 μF cm^{-2}) and averaged (≈26 μF cm^{-2}) values of measured capacitances were consistently higher than the 3–16 μF cm^{-2} capacitance range reported[20] for basal graphite sites but less than the 50–70 μF cm^{-2} evaluated for edge sites in 0.9 M NaF solutions. In CFRP, the production process of the carbon fibres and their uni-directional arrangement in the samples used in this work favour the presence of more edge sites on the exposed (transverse) ends of the carbon fibres in the CFRP samples, which might result in enhanced electrochemical activity of the CFRP. This explanation suggests that the electrochemical activity of CFRP samples with multi-directional carbon fibres is likely to be different.

With regard to cyclic voltametric investigations, the plot of modulus of $i_{p,a}$ vs. $v^{1/2}$ in Fig. 4b, is observed to be linear over a wide range of scan rates (and particularly at lower scan rates) suggestive of a reversible electron transfer process(es) involving freely diffusing redox species; a diffusion-controlled process[26,52]. Similar trend was also observed for the plot of modulus of $i_{p,c}$ vs. $v^{1/2}$ in Fig. 4b. Furthermore, the plot of i_p vs. v in Fig. 4c does not show similar linearity over a wide range of scan rates. Since the current response of electron transfer on an electrode involving adsorbed species is expected to have a linear relationship with the scan rate, a plot of the ratio of the anodic peak current to the cathodic peak current against the scan rate ($i_{p,a}/i_{p,c}$ vs. v, blue line in Fig. 4c) indicates equality at a scan rate of 1 mv s^{-1}, with the peak cathodic current increasing with increase in scan rates compared to the anodic peak current. The current ratios are observed to be closest to unity at scan rates from 1 to 100 mV s^{-1}. Above a scan rate of 100 mV s^{-1}, the anodic peak current ($I_{p,a}$) becomes increasing greater than the cathodic current ($I_{p,c}$). This observed trend of continuous increase in the magnitude of the anodic current peak as scan rate is increased (reduced relaxation time) is inferred to be related to increasing stability of the oxidized species in the progressively reducing time scales of the experiment which might be indicative of

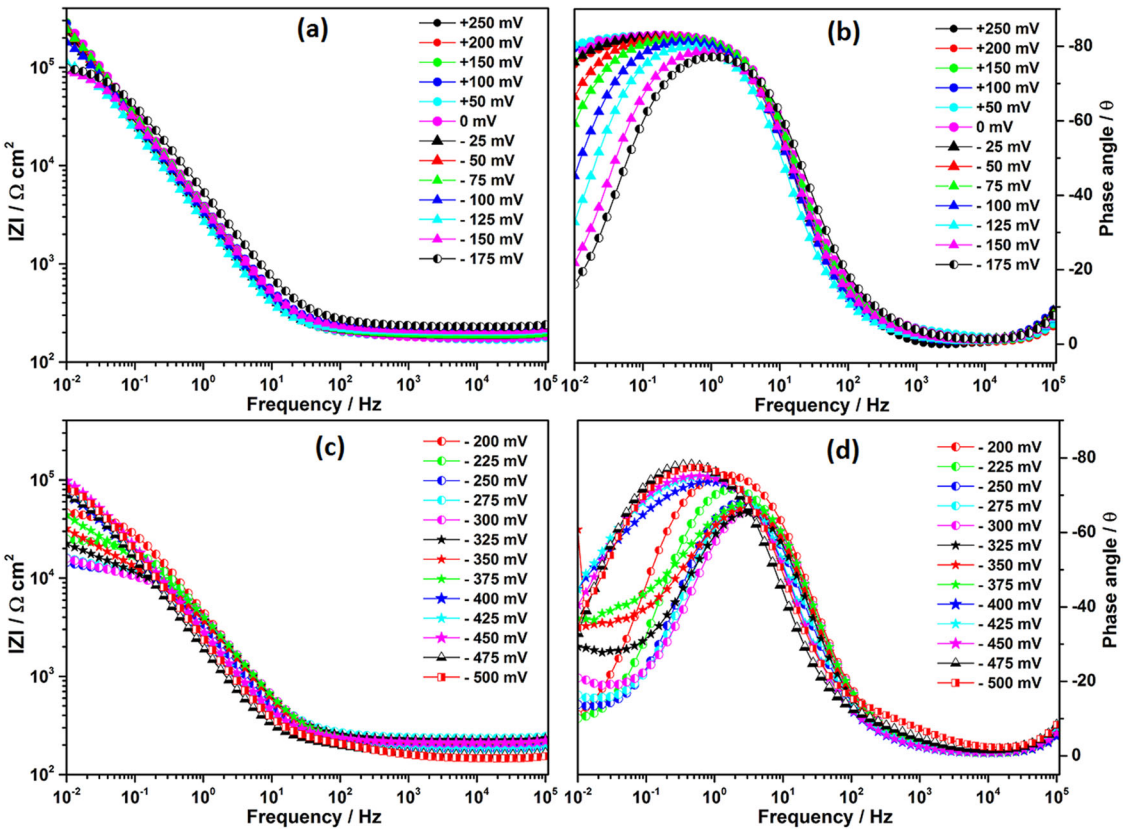

Fig. 9 Bode plots of CFRP at various polarizations. Bode plot of EIS spectra of CFRP in 50 mM NaCl at different polarizations between +250 and −500 mV_{SCE} to monitor diffusion effects.

some other interaction; most probably adsorption of some species on the CFRP surface. For this reason, rigorous analysis of cyclic voltammetry data in our work was limited to data acquired at scan speeds ≤100 mV s^{-1}. This interaction with carbon surfaces had been reported in earlier works[53,54] for ferri-ferrocyanide redox couple. Attributions have been made about formation of adsorbed intermediates on carbon surfaces during oxidation-reduction (electrochemical reactions) of ferri/ferrocyanide couples[54–57].

Concerning the electrochemically active surface areas, by employing the average of the electrochemically active surface areas (EASA) evaluated from cyclic voltammetry data (Table 1, last row), the relationship between the electrochemically active surface areas (EASA) and the geometric surface area (GSA) of 0.503 cm^2 as well as the assumed fraction of the GSA occupied by the carbon fibres was evaluated and presented in Table 2 based on data from scan speeds from 1 to 100 mV s^{-1} only. From the analysis of the cyclic voltammetry data (Table 2) it is possible to posit that the electrochemically active surface area (EASA) of the CFRP sample is most probably about 2.5 times larger than the geometric surface area (GSA) of the carbon fibre composite, and about four times larger than the assumed surface area of the carbon fibres (65% of its GSA) in the composite surface.

With respect to EIS studies, from Fig. 10 similar trends (as in Fig. 7 and Supplementary Fig. 3) are observed in the low frequency/global impedance (Fig. 10a), the capacitance (Fig. 10b), and the charge transfer resistance (Fig. 10c) over the selected potential range. However, marked differences in trends were observed at certain potential ranges. Figure 10c shows that from +150 mV_{SCE} (close to the OCP value of CFRP in the test media ≈ +125 mV_{SCE}) the charge transfer resistance (R_{ct}) decreases steeply with an increase in applied cathodic potentials until about −225 mV_{SCE}. In contrast, between −225 and −375 mV_{SCE} the charge transfer resistance (R_{ct}) is observed to be relatively stable. Interestingly, the resistive component ($W_{s\text{-}R}$ or R_d) of the diffusion impedance is observed to increase steeply in this same cathodic potential range (−225 to −375 mV_{SCE}); in which the charge transfer resistance (R_{ct}) appears to stabilize at is lowest values. Incidentally, this potential range (−225 to −375 mV_{SCE}) is consistent with the potential range of the cathodic peak observed in cyclic voltammetric tests (Fig. 7) attributed to the 2-electron reduction of oxygen with the formation of hydroxyl ions and hydrogen peroxide[9]. These observations can be explained by considering that an initial increase in the cathodic polarization stimulates the easier transfer of charges across the CFRP-solution interface causing the kinetics of the charge transfer process to be enhanced until the process comes under diffusion control. However, once diffusion control becomes dominant, the charge transfer resistance (R_{ct}) becomes independent of a further increase in applied cathodic potential, hence its value becomes lowered and stable with respect to applied potential. Similar trends are observed in the values of the global/low-frequency impedance (Fig. 10a) and capacitance (Fig. 10b) in this potential range (in which diffusion appears to predominate). At applied cathodic potentials <−450 mV_{SCE} (more negative) the impedance spectra no longer fit well to the 2-time constant equivalent circuit employed, which might be indicative of increased complexity in the operative electrochemical processes, as other cathodic processes besides the 2-electron oxygen reduction process apparently begin to become significant[3].

To confirm the hypothesis that the extracted fitting parameters were indeed related to diffusion affects the value 2.41×10^{-5} cm^2 s^{-1} obtained by Vivian and King[58] and considered by St-Denis and Fell[59,60] to be a reliable value for oxygen diffusion coefficient in water, the length of the diffusion layer was calculated from fitting and analysis of EIS data and presented as a function of potential in

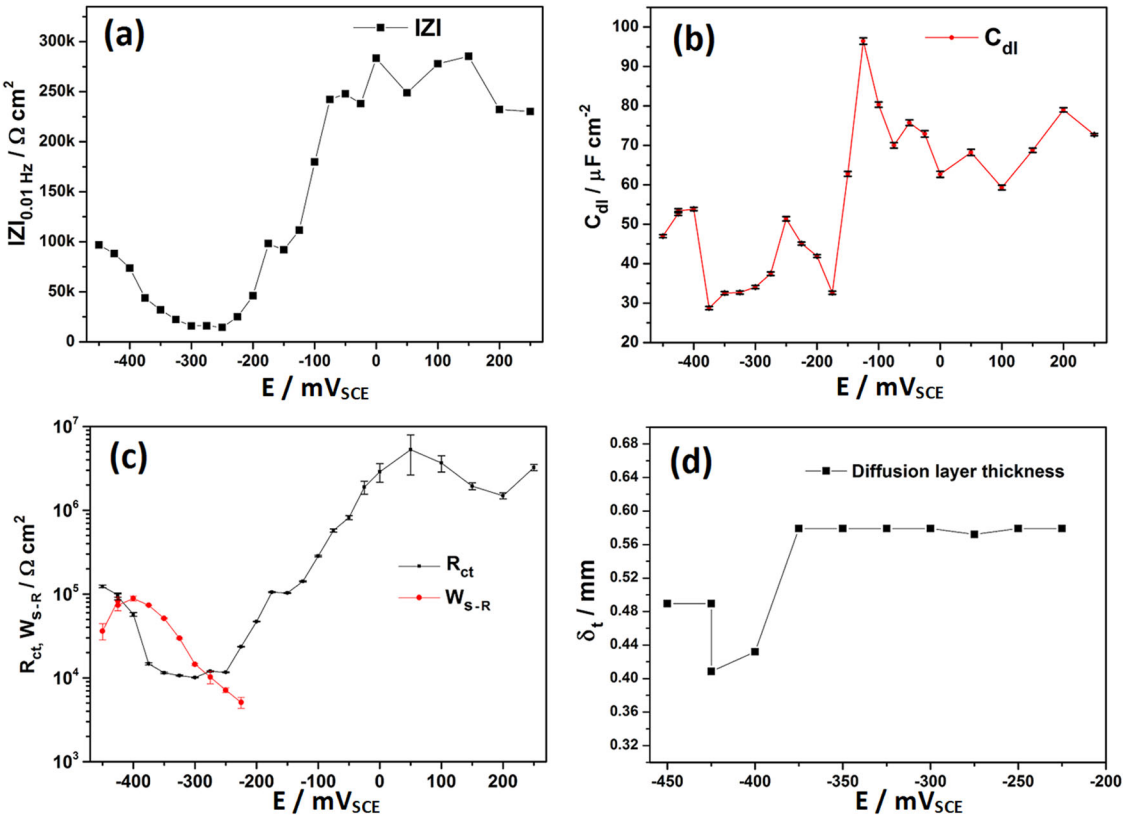

Fig. 10 Parameters for CFRP extracted from EIS at various polarizations. Parameters extracted from the EIS spectra as a function of potential around the diffusion-limited potential ranges for CFRP in 50 mM NaCl, **a** low-frequency impedance at 10^{-2} Hz, **b** calculated double-layer capacitances, **c** evolution of polarization or charge transfer resistance (R_{ct}), and the resistive component of Warburg impedance ($W_{S\text{-}R}$), and **d** the diffusion layer thickness estimated from EIS data (Error bars denote fitting errors from the model equivalent circuit used to fit data/extract parameter).

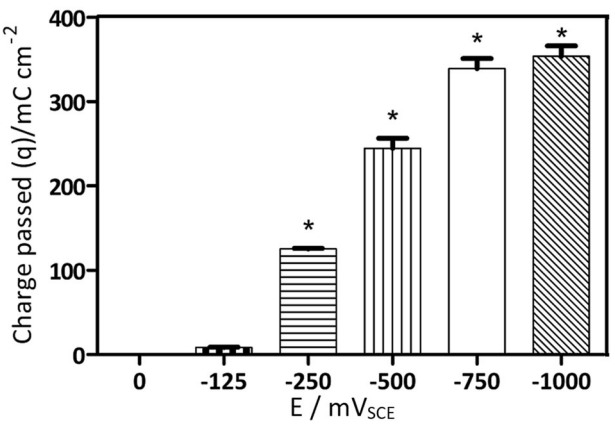

Fig. 11 Variation of charges passed per unit CFRP surface area with applied potential. Charges passed per unit of surface area in CFRP immersed in 50 m NaCl at different impressed potentials (from −1000 to 0 mV_{SCE}) during 4 h (Error bars within graph represent standard deviations of mean, asterisks denote potentials at which the specific charge passed were statistically significant ($P < 0.05$)).

Fig. 10d. From Fig. 10d, it can be observed that the calculated length of the diffusion layer is in the range of 0.42 to 0.58 mm and that the lower limit of calculated values are obtained at potentials more cathodic than −375 mV_{SCE}. Interestingly, it is above this potential value (≈−375 mV_{SCE}) that other cathodic processes besides the two-electron reduction process are deemed to most probably become significant. The fact that these values calculated from our EIS data for the diffusion layer thickness (δ) compare very well with values reported in unstirred electrolytes by Gerasimov and Rozenfeld[61] at 20 °C, which were 0.47 mm on platinum in 0.0047 N $FeCl_3$ + 0.1 N HCl, 0.52 mm on iron in 1 N NaCl solution, and 0.56 mm on copper in iron in 1 N NaCl solution, (and thus places the range of their reported values of diffusion layer thickness (δ) at 20 °C at 0.47–0.56 mm) confirms that the parameters extracted are consistent with diffusion effects. Discounting the lower values calculated for diffusion layer thickness at higher cathodic potentials where other processes besides two-electron oxygen reduction have been explained to become significant, the value of 0.58 mm calculated repeatedly at several potentials in the potential region in which the two-electron oxygen reduction predominates compare favourably with 0.56 mm reported on both iron and copper. The fact that the values of diffusion layer thickness (δ) calculated from treated EIS data compare so favourably with values reported from a different technique validates both the treatment of the EIS data and the inferences made from Fig. 10c, especially regarding the potential range in which the two-electron oxygen reduction predominates on CFRP surface. In addition, the fact that the diffusion layer thickness calculated from such a composite electrode with 6 μm diameter carbon fibres embedded in "seemingly" non-conductive epoxy matrix with the distances between neighbouring fibres seldom >12 μm (=2 carbon fibre diameters) (see insets in Figs. 2 and 13 for the microstructure of CFRP surface) compared favourably with values measured in monolithic metal surfaces is indicative that the CFRP surface appears to act electrochemically as a uniform and continuous electro-active surface when the diffusion-controlled processes dominate. This can be explained by the fact that the size of the carbon fibres (6 μm

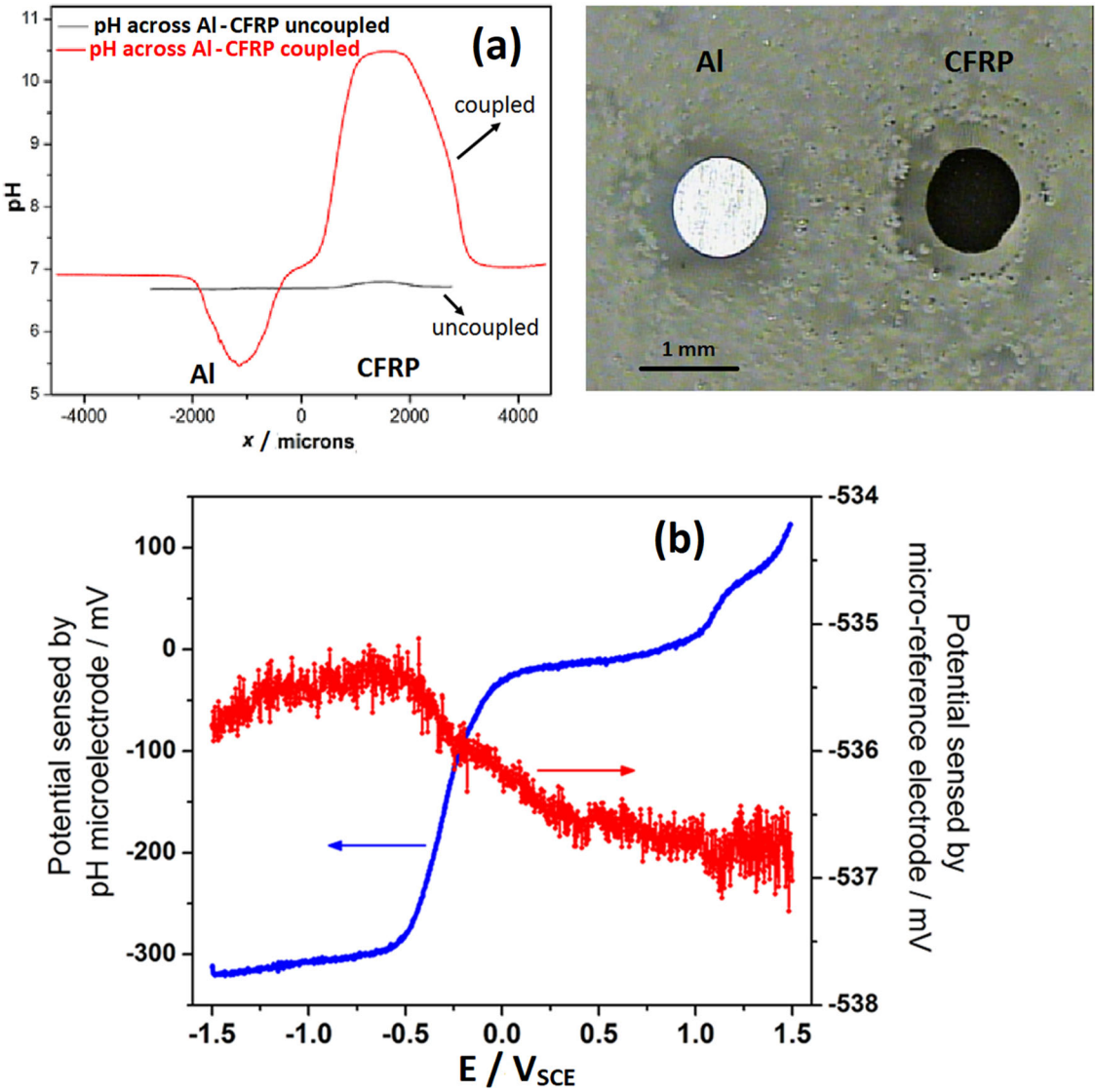

Fig. 12 Variation of local environment around Al and CFRP in Al-CFRP. Local environment information around CFRP and aluminium **a** pH profile across Al and CFRP galvanically coupled and uncoupled in 50 mM NaCl at 12 microns from the surface, and **b** potentials sensed by pH microelectrode and micro-reference electrode respectively at different applied potentials.

diameter) and the distance separating each carbon fibre from the other (≤12 µm) is much less than the estimated length of the diffusion layer 0.58 mm (=580 µm), the diffusion fields of adjacent carbon fibres are bound to overlap so that instead of acting as individual micro-electrodes, they apparently act as a single planar electrode under parallel diffusion limiting conditions[3].

Regarding the effect of observed changes under impressed polarization on CFRP degradation and corrosion of coupled metal (s), the observed reduction of pH over aluminium is most probably due to hydrolysis of aluminium ions. A comparison of this pH profile with that obtained by applying impressed cathodic polarization on CFRP (Fig. 5) in a similar potential range (at ≈−750 mV_{SCE} in both cases) shows that the pH above CFRP in both cases is <10. Such close agreement in the values of the local pH around CFRP on applying polarization by both methods validates the extensive use of impressed polarization of CFRP in this study.

Irrespective of the condition of the galvanically coupled CFRP surface (fresh or degraded) similar trends were observed in the galvanic potential and galvanic current evolution with time. However, for degraded CFRP galvanically coupled to aluminium in 50 mM NaCl solution the galvanic current density was in the range of 10–25 µA cm^{-2} and the galvanic potential in the range ≈−670 to −900 mV_{SCE}. These results (Fig. 13) indicate that prior degradation of CFRP does not enhance galvanic corrosion of coupled metal as the galvanic current density of the Al-CFRP couple with fresh CFRP surface (blue line in Fig. 13b) was consistently higher than that of Al-CFRP couple with CFRP surface that had undergone prior degradation (red line in Fig. 13b). Knowledge of these values would enable designers to focus on this realistic potential and current density ranges in the design and analysis of data from simulated polarization tests on CFRP. Furthermore, the fact that in spite of the increase in surface area of the conductive carbon fibres in the prior degraded CFRP due to prior exposure to alkaline pH buffer solution for 592 h (SEM image (s) in Fig. 13), galvanic corrosion of coupled metal was less than that for fresh CFRP coupled to metal suggests that other factors contribute more to galvanic corrosion than CFRP surface area. This lends credence to the strategy of mitigating galvanic corrosion of metals coupled to CFRP in multi-material assemblies by modification

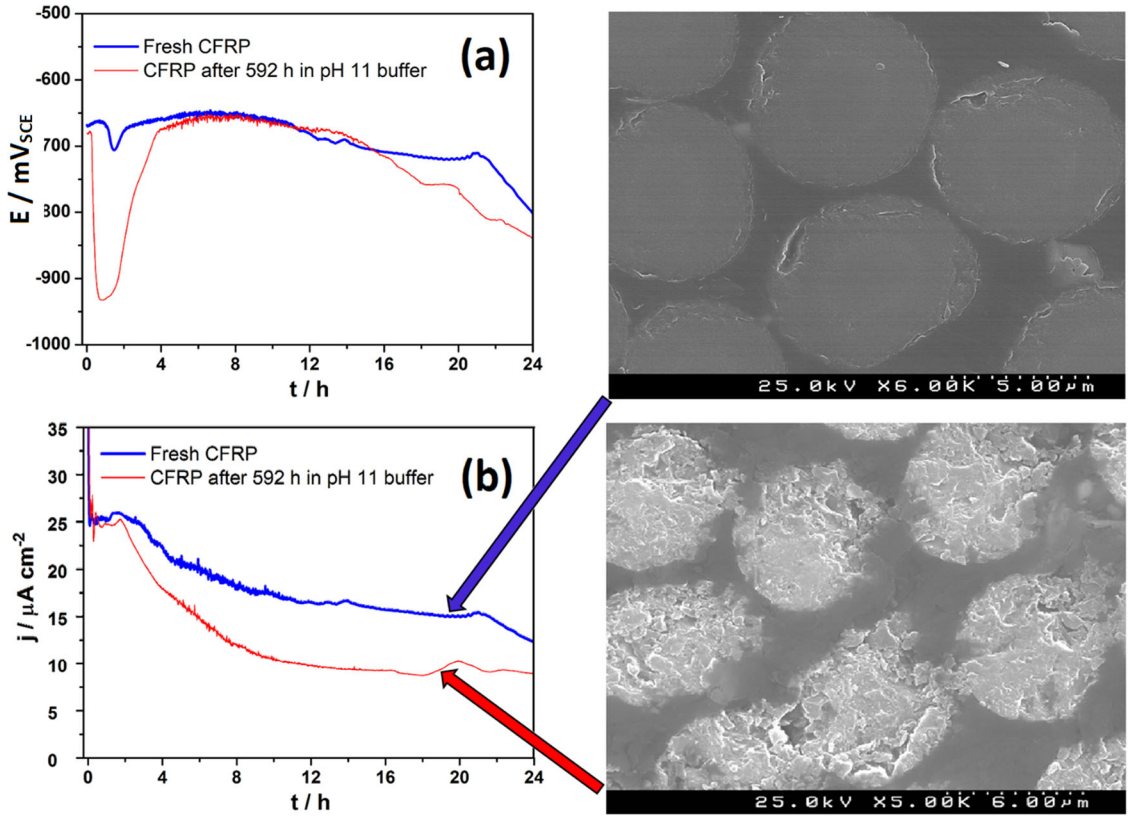

Fig. 13 Relationship between galvanic corrosion of Al-CFRP couples and condition of the CFRP surface. ZRA measurements of **a** potential and **b** galvanic current density profiles for Al-CFRP in 50 mM NaCl with freshly prepared CFRP surface and prior degraded CFRP sample, respectively (Inset are the SEM images of the fresh and degraded CFRP surfaces prior to ZRA measurements).

Table 2. Deduced EASA based on GSA of CFRP sample and its 65% carbon fibre content.

Data treatment conditions	Geometric surface area (GSA)	EASA	EASA: GSA	Considering 65% carbon fibre content EASA: GSA
Averaged values using scan rates from 1 to 100 mV s^{-1}	0.503 cm^2	1.29	2.57	3.93

of CFRP surface[51,62]. Results from this study suggest that the galvanic corrosion of coupled metal (Al) under the immersion conditions and partial or full diffusion control is not enhanced by prior degradation of coupled CFRP. However, the effect can be quite different when a thin film electrolyte with electrolyte thickness significantly lower than that of the diffusion layer is used. In that case the galvanic effect at a large distance between the CFRP and metal will not be significant, but the adjacent metal areas can be strongly affected[63–66]. This finding provides insight from a material degradation perspective that can be beneficial in component repair/replacement decisions in multi-material structures incorporating CFRP.

The apparent enhancement of the electrochemically active surface area (EASA) of the CFRP sample is principally attributed to the "microelectrode(s) effect". From duplicate measurements Galvanic current densities measured for Al-CFRP couple comprised of freshly polished CFRP sample in quiescent 50 mM NaCl ranged from 15 to 25 μA cm^{-2} and ≈−660 to −850 mV$_{SCE}$ respectively, while the corresponding parameter for Al-CFRP couple comprised of degraded CFRP sample was in the range 10–25 μA cm^{-2} and ≈−670 to −900 mV$_{SCE}$, while the pH above CFRP surface in the couple is ≥10. Results confirm the intense electrochemical activity of CFRP even when slightly polarized cathodically with a concomitant sharp increase in the pH above its surface. Since CFRP is cathodically polarized when galvanically coupled to many metals (e.g, iron, tin, aluminium, zinc and magnesium), enhanced corrosion of multi-material structures incorporating CFRP is favoured in the presence of moisture. However, since this activity comes with a significant change in pH and will most probably provoke a balancing anodic activity in the metal, it might be feasible to employ inhibitors triggered by the rapid increase in pH around the metal-CFRP junction to mitigate corrosion in the metal component(s) of galvanically coupled composite/hybrid structures. Contrary to expectations, results indicate that prior exposure of CFRP to degradative high pH media, before galvanic coupling does not provoke accelerated galvanic corrosion of the coupled metal under bulk electrolyte immersion conditions.

METHODS

Materials preparation

Pultruded CFRP rods of diameters 1 and 8 mm with 65% fibre content, made of Tenax HT 24 K carbon fibre, and epoxy vinyl matrix material were obtained from Modulor Material Total GmbH[67]. These were cut to required lengths, and mounted in a polymeric resin (Epokwick from Buehler, USA)

after attaching a conductive wire at one end for electrical contact. Before each test, the fresh surface was exposed by wet-grinding progressively with silicon carbide paper of grit sizes, 240, 360, 400, 500, 600 and 1200, washing in between with copious amounts of distilled water.

Test procedures

Most of the electrochemical tests were carried out using Autolab PGSTAT302N potentiostat, employing the three-electrode method with a saturated calomel reference electrode, platinum wire as counter electrode and (CFRP) as the working electrode. For the measurements involving "microelectrodes" (pH measurements with simultaneous potentiodynamic polarization), an Ivium Compactstat potentiostat was used. For galvanic corrosion evaluation, a Gamry Interface 1000 Potentiostat/Galvanostat/ZRA equipment was used.

Open circuit potential measurements

Using the three-electrode arrangement open circuit potential of the CFRP in 50 mM NaCl test solutions was monitored at 60 s intervals immediately after immersion till 10 h.

Potentiodynamic tests

Triplicate potentiodynamic tests were carried on CFRP in quiescent 50 mM NaCl test solutions with a potential step size of 1 mV and a scan rate of 1 mV s^{-1} after 1-h immersion at OCP (without any conditioning), from 20 mV anodic of OCP till −2000 mV_{SCE}.

Chronoamperometric measurements

Using the three-electrode arrangement triplicate chronoamperometric tests were carried out on CFRP polarized to −1000, −750, −500, −250, −125, and 0 mV_{SCE}, respectively in quiescent 50 mM NaCl solution for 4 h with current sampled every 15 s along with the quantity of charge passed during the test duration.

Electrochemical impedance spectroscopy

Electrochemical impedance spectroscopy was done using a single sine wave of 10 mV (RMS) amplitude in the frequency range of 100,000 Hz to 10 mHz after 1-h immersion in the test solutions at OCP, and at −1000, −500, +250, and +500 mV_{SCE} after conditioning during the 1-h immersion periods at the 5 respective potentials. To check the effect of time on the impedance spectra, these tests were repeated after 2-, 4-, 6-, 8-, and 10-h immersion and conditioning at the respective potentials.

pH measurements

The pH was measured using equipment and procedure reported elsewhere[68], at a height of 40 micron along a straight line cutting through 2 mm diameter CFRP and aluminium rods galvanically coupled together by a method reported elsewhere[68]. Point pH measurements were made 40 µm above the surface of a 2 mm diameter CFRP rod immersed in 50 mM NaCl while simultaneously making a polarization scan from −1500 to 1500 mV_{SCE} at a scan rate of 1 mV s^{-1} and step size of 1 mV. Furthermore, pH was measured as the potential is varied stepwise from cathodic to anodic values.

Cyclic voltammetry

Employing the well-known Ferricyanide/Ferrocyanide redox couple, a cyclic voltammetry study of the electrode behaviour of CFRP in 0.1 M KCl + 1mM $K_4[Fe(CN)_6]$ + 1mM $K_3[Fe(CN)_6]$ was done at different scan rates between −200 and +500 mV_{SCE}, using a three-electrode arrangement and a step size of 2 mV. In addition, repeated cyclic scans were made in 50 mM NaCl over an enhanced potential window (−1500 to +1500 mV_{SCE}).

DATA AVAILABILITY

All data generated or analysed during this study are included in this published article (and its Supplementary Information files).

Received: 19 February 2022; Accepted: 5 June 2022;
Published online: 29 June 2022

REFERENCES

1. Miller Jr, B. A. The galvanic corrosion of graphite epoxy composite materials coupled with alloys (No. GAE/MC/75D-8). https://apps.dtic.mil/dtic/tr/fulltext/u2/a019322.pdf (1975).
2. Mandel, M. & Krüger, L. Electrochemical corrosion studies and pitting corrosion sensitivity of a self-pierce rivet joint of carbon fibre reinforced polymer (CFRP)–laminate and EN AW-6060-T6. *Mater. Werkst.* **43**, 302–309 (2012).
3. Ofoegbu, S.U. *Corrosion and Corrosion Inhibition in Multi-material Combinations*. PhD Thesis, University of Aveiro, Portugal. (2018).
4. Tavakkolizadeh, M. & Saadatmanesh, H. Galvanic corrosion of carbon and steel in aggressive environments. *J. Compos. Constr.* **5**, 200–210 (2001).
5. Tucker, W. C., Brown, R. & Russell, L. Corrosion between a graphite/polymer composite and metals. *J. Compos. Mater.* **24**, 92–102 (1990).
6. Miriyala, S., Tucker, W., Rockett, T. & Brown, R. Degradation of carbon reinforced polymer composites under galvanic coupling conditions. In *33rd Structures, Structural Dynamics and Materials Conference*. (1992).
7. Kaushik, D., Alias, M. N. & Brown, R. An impedance study of a carbon fiber/vinyl ester composite. *Corrosion* **47**, 859–867 (1991).
8. Sloan, F. E. & Talbot, J. B. Corrosion of graphite-fiber-reinforced composites I-galvanic coupling damage. *Corrosion* **48**, 830–838 (1992).
9. Alias, M. N. & Brown, R. Damage to composites from electrochemical processes. *Corrosion* **48**, 373–378 (1992).
10. Woo, E. M., Chen, J. S. & Carter, C. S. Mechanisms of degradation of polymer composites by galvanic reactions between metals and carbon fiber. *Polym. Compos.* **14**, 395–401 (1993).
11. Sloan, F. E. & Talbot, J. B. Corrosion of graphite-fiber-reinforced composites II-anodic polarization damage. *Corrosion* **48**, 1020–1026 (1992).
12. Shapoval, G. S., Pud, A. A., Zamotayev, P. V. & Kachan, A. A. Degradation of some carbon-chain polymers by electrochemical reduction. *Poly. Sci.* **27**, 2427–2431 (1985).
13. Tucker, W. C. Degradation of graphite/polymer composites in seawater. *J. Energy Resour. Technol.* **113**, 264–267 (1991).
14. Tucker, W. C., Brown, R., Rockett, T. J., & Miriyala, S. K. Blistering of graphite/polymer composites galvanically coupled with metals in sea water. https://apps.dtic.mil/sti/pdfs/ADA257247.pdf (1992).
15. Alias, M. N. & Brown, R. Corrosion behavior of carbon fiber composites in the marine environment. *Corros. Sci.* **35**, 395–402 (1993).
16. Tang, Y., Hartt, W., Granata, R., Yu, H. & Farooq, M. U. Degradation of carbon/vinyl ester composites under cathodic polarization in seawater. *J. Compos. Mater.* **46**, 3115–3120 (2012).
17. Bauer, A., Grundmeier, G., Steger, H. & Weitl, J. Corrosive delamination processes of CFRP-aluminum alloy hybrid components. *Werkst. Korros.* **69**, 98–105 (2018).
18. Kinoshita K. & Chu X. Carbon for supercapacitors, in *Proc. Symp. on Electrochemical Capacitors*, (The Electrochemical Society, 1996),
19. Kinoshita, K. *Carbon: Electrochemical and Physicochemical Properties* (Wiley, 1988).
20. Frackowiak, E. & Beguin, F. Carbon materials for the electrochemical storage of energy in capacitors. *Carbon* **39**, 937–950 (2001).
21. Brownson, D. A., Munro, L. J., Kampouris, D. K. & Banks, C. E. Electrochemistry of graphene: not such a beneficial electrode material? *RSC Adv.* **1**, 978–988 (2011).
22. Brownson, D. A., Kampouris, D. K. & Banks, C. E. Graphene electrochemistry: fundamental concepts through to prominent applications. *Chem. Soc. Rev.* **41**, 6944–6976 (2012).
23. Yuan, W. et al. The edge-and basal-plane-specific electrochemistry of a single-layer graphene sheet. *Sci. Rep.* **3**, 2248 (2013).
24. Randin, J. P. & Yeager, E. Differential capacitance study of stress-annealed pyrolytic graphite electrodes. *J. Electrochem. Soc.* **118**, 711–714 (1971).
25. Brug, G. J., Van Den Eeden, A. L. G., Sluyters-Rehbach, M. & Sluyters, J. H. The analysis of electrode impedances complicated by the presence of a constant phase element. *J. Electroanal. Chem. Interfacial Electrochem.* **176**, 275–295 (1984).
26. Elgrishi, N. et al. A practical beginner's guide to cyclic voltammetry. *Chem. Educ.* **95**, 197–206 (2018).
27. Hood, S. J. et al. Why 'the bigger the better'is not always the case when utilising microelectrode arrays: high density vs. low density arrays for the electroanalytical sensing of chromium (VI). *Analyst* **134**, 2301–2305 (2009).
28. Zhu, F., Mao, B. & Yan, J. Double electrode systems with microelectrode arrays for electrochemical measurements. *Rev. Anal. Chem.* **34**, 87–101 (2015).
29. Davies, T. J. & Compton, R. G. The cyclic and linear sweep voltammetry of regular and random arrays of microdisc electrodes: theory. *J. Electroanal. Chem.* **585**, 63–82 (2005).
30. Davies, T. J. et al. The cyclic and linear sweep voltammetry of regular arrays of microdisc electrodes: fitting of experimental data. *J. Electroanal. Chem.* **585**, 51–62 (2005).
31. Chen, R., Li, Y., Huo, K. & Chu, P. K. Microelectrode arrays based on carbon nanomaterials: emerging electrochemical sensors for biological and environmental applications. *RSC Adv.* **3**, 18698–18715 (2013).

32. Stulík, K., Amatore, C., Holub, K., Marecek, V. & Kutner, W. Microelectrodes. Definitions, characterization, and applications (Technical report). *Pure Appl. Chem.* **72**, 1483–1492 (2000).
33. Patel, P. R. et al. Chronic in vivo stability assessment of carbon fiber microelectrode arrays. *J. Neural Eng.* **13**, 066002 (2016).
34. Huang, X. J., O'Mahony, A. M. & Compton, R. G. Microelectrode arrays for electrochemistry: approaches to fabrication. *Small* **5**, 776–788 (2009).
35. Gardner, R. D., Zhou, A. & Zufelt, N. A. Development of a microelectrode array sensing platform for combination electrochemical and spectrochemical aqueous ion testing. *Sens. Actuators B Chem.* **136**, 177–185 (2009).
36. Ino, K., Shiku, H. & Matsue, T. Bioelectrochemical applications of microelectrode arrays in cell analysis and engineering. *Curr. Opin. Electrochem.* **5**, 146–151 (2017).
37. Jin, Y. et al. Fabrication of surface renewable carbon microelectrode arrays and their application in heavy metal ion sensing. *Anal. Methods* **11**, 1284–1288 (2019).
38. Lin, Z. et al. An addressable microelectrode array for electrochemical detection. *Anal. Chem.* **80**, 6830–6833 (2008).
39. Kim, R., Joo, S., Jung, H., Hong, N. & Nam, Y. Recent trends in microelectrode array technology for in vitro neural interface platform. *Biomed. Eng. Lett.* **4**, 129–141 (2014).
40. Liu, Y., Li, X., Chen, J. & Yuan, C. Micro/nano electrode array sensors: advances in fabrication and emerging applications in bioanalysis. *Front. Chem.* **8**, 573865 (2020).
41. Yang, H., Rahman, M. T., Du, D., Panat, R. & Lin, Y. 3-D printed adjustable microelectrode arrays for electrochemical sensing and biosensing. *Sens. Actuators B Chem.* **230**, 600–606 (2016).
42. Stett, A. et al. Biological application of microelectrode arrays in drug discovery and basic research. *Anal. Bioanal. Chem.* **377**, 486–495 (2003).
43. Xu, L. et al. Trends and recent development of the microelectrode arrays (MEAs). *Biosens. Bioelectron*. **179**, 112854 (2021).
44. Taylor, R. J. & Humffray, A. A. Electrochemical studies on glassy carbon electrodes. *J. Electroanal. Chem. Interfacial Electrochem.* **64**, 63–84 (1975).
45. Šljukić, B., Banks, C. E., Mentus, S. & Compton, R. G. Modification of carbon electrodes for oxygen reduction and hydrogen peroxide formation: the search for stable and efficient sonoelectrocatalysts. *Phys. Chem. Chem. Phys.* **6**, 992–997 (2004).
46. Šljukić, B., Banks, C. E. & Compton, R. G. An overview of the electrochemical reduction of oxygen at carbon-based modified electrodes. *J. Iran. Chem. Soc.* **2**, 1–25 (2005).
47. Lin, C. J., Du, R. G. & Nguyen, T. In-situ imaging of chloride ions at the metal/solution interface by scanning combination microelectrodes. *Corrosion* **56**, 41–47 (2000).
48. Denuault, G., Frank, M. T. & Peter, L. M. Scanning electrochemical microscopy: potentiometric probing of ion fluxes. *Faraday Discuss.* **94**, 23–35 (1992).
49. Bastos, A. in *Handbook of Sol-Gel Science and Technology* 2nd edn. (Klein, L., Aparicio, M. & Jitianu, A. eds) pp. 1–57 (Springer International Publishing AG, 2017).
50. Kiss, A., Filotás, D., Souto, R. M. & Nagy, G. The effect of electric field on potentiometric scanning electrochemical microscopic imaging. *Electrochem. Commun.* **77**, 138–141 (2017).
51. Ofoegbu, S. U., Ferreira, M. G. & Zheludkevich, M. L. Galvanically stimulated degradation of carbon-fiber reinforced polymer composites: a critical review. *Materials* **12**, 651 (2019).
52. Bard, A. J. & Faulkner, L. R. *Electrochemical Methods Fundamentals and Applications* 1st edn. (Wiley, 1980).
53. Granger, M. C. & Swain, G. M. The influence of surface interactions on the reversibility of Ferri/Ferrocyanide at boron-doped diamond thin-film electrodes. *J. Electrochem. Soc.* **146**, 4551–4558 (1999).
54. Pharr, C. M. & Griffiths, P. R. Infrared spectroelectrochemical analysis of adsorbed hexacyanoferrate species formed during potential cycling in the ferrocyanide/ferricyanide redox couple. *Anal. Chem.* **69**, 4673–4679 (1997).
55. Zhang, J., Yin, Q., Cai, S. & Fujishima, A. In situ fourier transform infrared reflection spectroscopic studies of ferricyanide/ferrocyanide on graphite electrode. *Electroanalysis* **5**, 517–520 (1993).
56. Chen, P. & McCreery, R. L. Control of electron transfer kinetics at glassy carbon electrodes by specific surface modification. *Anal. Chem.* **68**, 3958–3965 (1996).
57. Kamoshida, N. et al. In situ ATR-IR study of $Fe(CN)_6^{3-}$/$Fe\ CN)_6^{4-}$ redox system on boron-doped diamond electrode. Diam.Relat. Mater. 93, 50–53 (2019).
58. Vivian, J. E. & King, C. J. Diffusivities of slightly soluble gases in water. *AIChE J.* **10**, 220–221 (1964).
59. St-Denis, C. E. & Fell, C. J. D. Diffusivity of oxygen in water. *Can. J. Chem. Eng.* **49**, 885–885 (1971).
60. Tse, F. C. & Sandall, O. C. Diffusion coefficients for oxygen and carbon dioxide in water at 25 °C by unsteady state desorption from a quiescent liquid. *Chem. Eng. Commun.* **3**, 147–153 (1979).
61. Gerasimov, V. V. & Rozenfeld, I. L. Effect of temperature on the diffusion current and the thickness of the diffusion layer. *Russ. Chem. Bull.* **5**, 797–801 (1956).
62. Ofoegbu, S. U. et al. Modification of carbon fibre reinforced polymer (CFRP) surface with sodium dodecyl sulphate for mitigation of cathodic activity. *Appl. Surf. Sci.* **478**, 924–936 (2019).
63. Palani, S., Hack, T., Deconinck, J. & Lohner, H. Validation of predictive model for galvanic corrosion under thin electrolyte layers: an application to aluminium 2024-CFRP material combination. *Corros. Sci.* **78**, 89–100 (2014).
64. Dolgikh, O., Bastos, A. C., Oliveira, A., Dan, C. & Deconinck, J. Influence of the electrolyte film thickness and NaCl concentration on the oxygen reduction current on platinum. *Corros. Sci.* **102**, 338–347 (2016).
65. Liu, C., Srinivasan, J. & Kelly, R. G. Electrolyte film thickness effects on the cathodic current availability in a galvanic couple. *J. Electrochem. Soc.* **164**, C845–C855 (2017).
66. Bouali, A. C. et al. Evaporation of electrolyte during SVET measurements: the scale of the problem and the solutions. *Electroanalysis* **31**, 2290–2298 (2019).
67. Modulor GmbH. Pultruded carbon fibre (CRP) rod, round https://www.modulor.de/en/pultruded-carbon-fibre-crp-rod-round.html (2016).
68. Bastos, A. C., Karavai, O. V., Zheludkevich, M. L., Yasakau, K. A. & Ferreira, M. G. S. Localised measurements of pH and dissolved oxygen as complements to SVET in the investigation of corrosion at defects in coated aluminum alloy. *Electroanalysis* **22**, 2009–2016 (2010).

ACKNOWLEDGEMENTS

Funding from FCT project: "Corrosion and Corrosion Protection in Multi-material Systems", (PTDC/CTM/108446/2008), and European FP7 project: "Active PROtection of multi-material assemblies for AIRcrafts" ["PROAIR" (PIAPP-GA-2013-612415)] are acknowledged. S.U.O. acknowledges Fundação para a Ciência e a Tecnologia (FCT) Portugal for doctoral (SFRH/BD/75167/2010) grant. This work was developed within the scope of the project CICECO-Aveiro Institute of Materials, POCI-01-0145-FEDER-007679 (FCT Ref. UID /CTM /50011/2013), financed by national funds through the FCT/MEC and when appropriate co-financed by FEDER under the PT2020 Partnership Agreement. This work was also supported by the projects UIDB/00481/2020 - FCT - Fundação para a Ciencia e a Tecnologia; and CENTRO-01-0145-FEDER-022083 - Centro Portugal Regional Operational Programme (Centro2020), and POCI-OT1-PI 1.2-TI 47-FEDER-033912—Competitiveness and Internationalization Operational Program, under the PORTUGAL 2020 Partnership Agreement, through the European Regional Development Fund.

AUTHOR CONTRIBUTIONS

All authors made substantial contributions to the conception of the work, acquisition, analysis and interpretation of data. All authors also approved the submitted version and agreed to be both personally accountable for the author's own contributions and to ensure that questions related to the accuracy or integrity of any part of the work, even ones in which the author was not personally involved, are appropriately investigated, resolved, and the resolution documented in the literature. The particular contributions of each author is enumerated as follows; S.U.O.: conceptualization, investigation, methodology, formal analysis, writing—original and subsequent drafts. M.C.Q.: investigation, data acquisition and treatment. A.C.B.: investigation, data acquisition and treatment, internal review of drafts. M.G.S.F.: formal analysis, and supervision, internal review of drafts and editing. M.L.Z.: conceptualization, formal analysis, and supervision, internal review of drafts, and funding acquisition.

COMPETING INTERESTS

The authors declare no competing interests.

ADDITIONAL INFORMATION

Supplementary information The online version contains supplementary material available at https://doi.org/10.1038/s41529-022-00261-1.

Correspondence and requests for materials should be addressed to Stanley Udochukwu Ofoegbu.

Reprints and permission information is available at http://www.nature.com/reprints

Publisher's note Springer Nature remains neutral with regard to jurisdictional claims in published maps and institutional affiliations.